


Chitosan Nerve Grafts Incorporated with SKP-SC-EVs Induce Peripheral Nerve Regeneration

Xinyang Zhou^{1,2} · Miaomei Yu^{2,3} · Daiyue Chen² · Chunyan Deng² · Qi Zhang² · Xiaosong Gu² · Fei Ding² 

Received: 15 November 2022 / Revised: 20 December 2022 / Accepted: 25 December 2022 / Published online: 6 March 2023
© Korean Tissue Engineering and Regenerative Medicine Society 2023

Abstract

BACKGROUND: Repair of long-distance peripheral nerve defects remains an important clinical problem. Nerve grafts incorporated with extracellular vesicles (EVs) from various cell types have been developed to bridge peripheral nerve defects. In our previous research, EVs obtained from skin-derived precursor Schwann cells (SKP-SC-EVs) were demonstrated to promote neurite outgrowth in cultured cells and facilitate nerve regeneration in animal studies.

METHODS: To further assess the functions of SKP-SC-EVs in nerve repair, we incorporated SKP-SC-EVs and Matrigel into chitosan nerve conduits (EV-NG) for repairing a 15-mm long-distance sciatic nerve defect in a rat model. Behavioral analysis, electrophysiological recording, histological investigation, molecular analysis, and morphometric assessment were carried out.

RESULTS: The results revealed EV-NG significantly improved motor and sensory function recovery compared with nerve conduits (NG) without EVs incorporation. The outgrowth and myelination of regenerated axons were improved, while the atrophy of target muscles induced by denervation was alleviated after EVs addition.

CONCLUSION: Our data indicated SKP-SC-EVs incorporation into nerve grafts represents a promising method for extended peripheral nerve damage repair.

Keywords Extracellular vesicles from skin-derived precursor Schwann cells (SKP-SC-EVs) · Chitosan · Peripheral nerve regeneration

Xinyang Zhou, Miaomei Yu are contributed equally.

✉ Fei Ding
dingfei@ntu.edu.cn

¹ School of Biology and Basic Medical Sciences, Soochow University, Suzhou, China

² Key Laboratory of Neuroregeneration of Jiangsu and Ministry of Education, Co-Innovation Center of Neuroregeneration, NMPA Key Laboratory for Research and Evaluation of Tissue Engineering Technology Products, Jiangsu Clinical Medicine Center of Tissue Engineering and Nerve Injury Repair, Nantong University, 19 Qixiu Road, Nantong 226001, Jiangsu, China

³ Clinical Medical Research Center, The Third Affiliated Hospital of Soochow University, Changzhou, China

1 Introduction

Many conditions, including accidents, surgery, infections, and congenital diseases, cause peripheral nerve injuries (PNI), leading to deficits in motor and sensory neuronal functions. With the development of biomaterials and tissue engineering, short-distance peripheral nerve injuries may be managed by surgical procedures or nerve graft transplantation, while long-distance (over 10 and 30 mm in the rat and human species, respectively) nerve defects remain difficult to repair and neural function can hardly recover [1, 2]. Clinically, the present gold standard for treating long-distance nerve defects is still bridging the defects with autologous nerve graft although accompanied by many problems, including new trauma, limited supply, and

mismatch with the injury site [3, 4]. To avoid these limitations, nerve grafts (NGs) have been developed to become an alternative tool for PNI repair. In addition, strategies to enhance axonal regeneration by the addition of Schwann cells (SCs), stem cells, or growth factors have been applied to promote regeneration in nerve injuries with extended defect sizes [1, 2, 5–8].

Many natural or synthetic materials, including collagen, chitosan, gelatin, cellulose, polylactic acid, polycaprolactone, and hyaluronic acid, have been used to construct nerve guide conduits (NGCs) for replacing autologous NGs for peripheral nerve reconstruction [9, 10]. Various technologies have been developed to prepare NGCs, including electrospinning, solvent casting, gas foaming, decellularization, micropatterns, and three-dimensional (3D) printing [11–15]. Many ameliorations in materials, design and production methods have been proposed to obtain ideal NGCs to generate diverse mechanical, biological, and biochemical hints for nerve regeneration [16].

Chitosan is a natural, lowly toxic, antibacterial, highly biocompatible, and biodegradable bioactive polymer. Not only chitosan-built NGs provide appropriate scaffolds for nerve regeneration, but also their catabolites facilitate nerve repair by re-constructing a microenvironment for nerve regeneration [17]. A chitin/CM-chitosan artificial NG was reported to successfully repair 10-mm rat sciatic nerve defects [18]. Filling the longitudinal chitosan film in chitosan nerve conduits could significantly improve nerve regeneration functionally and morphologically in 15-mm sciatic nerve defects in rats, indicating that chitosan has the potential to be used in repairing long-distance nerve defects [19]. The incorporation of growth factors is another strategy for improving nerve regeneration in long-distance nerve defects. Aligned chitosan fiber hydrogel with bioactive peptide mimicking brain-derived neurotrophic factor (BDNF) and vascular endothelial growth factor (VEGF) was reported to induce nerve regeneration and vascular penetration in 15-mm rat sciatic nerve defects [7].

Extracellular vesicles (EVs) are responsible for intercellular communication and information transduction, and are considered to play fundamental roles in the pathophysiological events in the nervous system [20]. Skin-derived precursor Schwann cells (SKP-SCs) were easily accessible and showed promotive effects in nerve regeneration and myelination [21]. SKP-SC-derived acellular matrix was utilized to modify chitosan/silk scaffolds to repair a rat sciatic nerve defect [22], indicating SKP-SCs as a potential source of glial cells for enhancing peripheral nerve regeneration.

In a previous report, we designed an artificial NG via injection of SKP-SC-EVs-encapsulating Matrigel into a silicone conduit, which was employed for bridging 10-mm long sciatic nerve defects in rats [23]. Here, we designed an

NG by incorporation of SKP-SC-EVs in chitosan conduits, and its effect was evaluated on the functional and morphological recovery of 15-mm sciatic nerve defects in a rat model.

2 Materials and methods

2.1 Materials

DMEM/F12 and fetal bovine serum (FBS) were provided by Gibco (Grand Island, NY, USA). Forskolin, chloral hydrate, pentobarbital sodium, PKH26, anti-NF200, anti-CD81, and α -bungarotoxin (α -BTX) were provided by Sigma (St. Louis, MO, USA). TRIzol reagent was from Invitrogen (Carlsbad, CA, USA). SYBR green mix was from Vazyme (Nanjing, China). Heregulin-1 β was provided by R&D Systems (Minneapolis, MN, USA). N2 supplement was from StemCell Technologies (Canada); penicillin/streptomycin (P/S), Hoechst 33,258, and 4',6-diamidino-2-phenylindole (DAPI) were from Beyotime Biotechnology (Shanghai, China). Omniscript RT kit and ExoEasy Maxi Kit were from Qiagen (Germantown, MD, USA). Fluorogold TM was from Biotium (Fremont, CA, USA). Anti-Alix and anti-tumor susceptibility gene 101 (TSG101) were from Proteintech (Rosemont, IL, USA). Anti-Laminin, Alexa Fluor 594-linked anti-rabbit IgG, and Alexa Fluor 488-linked anti-rabbit IgG secondary antibodies were provided by Abcam (Cambridge, MA, USA). The chitosan conduit ($\phi 2 \times 3$ mm; length, 15 mm) was from Eton (Nanjing, China). Masson's trichrome staining kit was provided by Solarbio (Beijing, China).

2.2 Preparation and characterization of SKP-SC-EVs

SKP-SCs were cultured as described previously [24]. The culture medium was DMEM/F12 (3:1) with 3% FBS, 2% N2 supplement, 50 ng/ml heregulin-1 β , 5 μ M forskolin, and 1% P/S. Before the isolation of EVs from SKP-SCs, the cells were washed with PBS and further incubated in a serum-free medium for 48 h. Then, the culture medium was obtained, and SKP-SC-EVs were purified from supernatants with the ExoEasy Maxi Kit according to the protocol proposed by the manufacturer.

The characterization of SKP-SC-EVs was carried out by nanoparticle tracking analysis (NTA), transmission electron microscopy (TEM), and Western blot as described previously [23, 24]. The primary antibodies applied included: anti-CD81 (1:1000), anti-Alix (1:1000), anti-TSG101 (1:1000), and anti-Calnexin (1:1000).

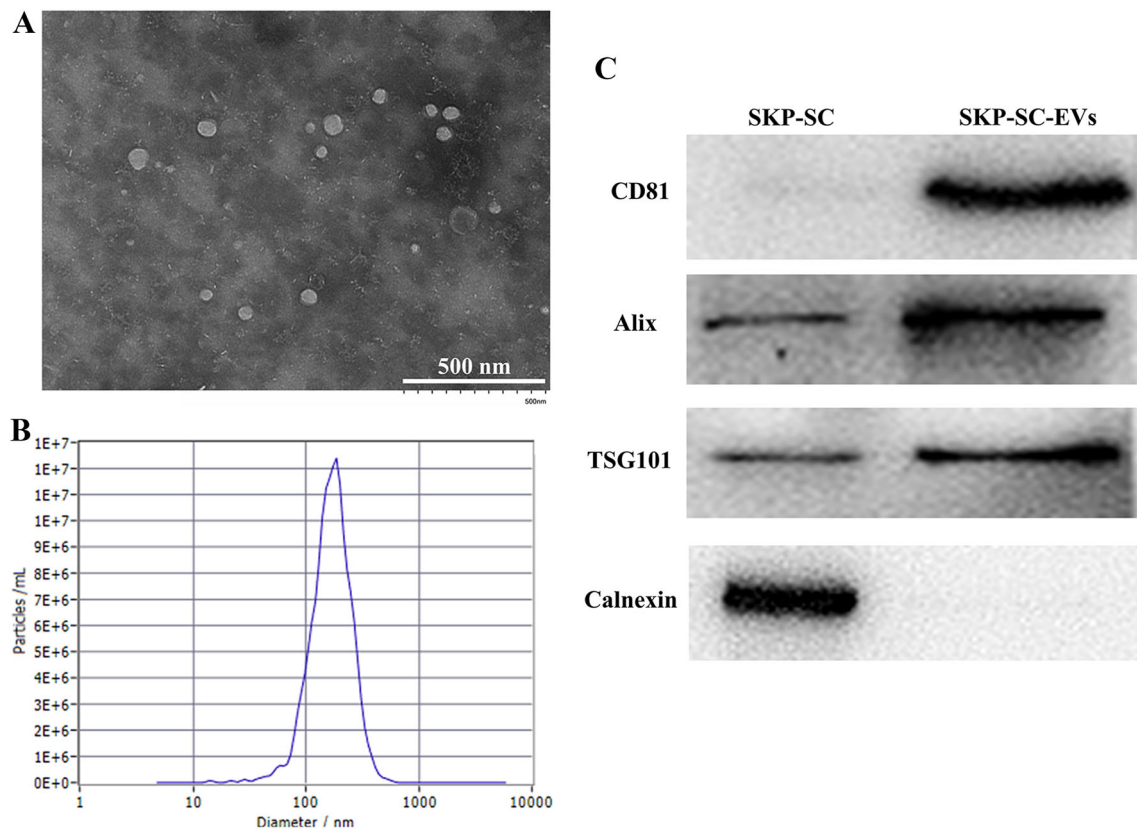


Fig. 1 The characterization SKP-SC-EVs. **A** Transmission electron microscopy (TEM) of SKP-SC-EVs the typical cup-shape of EVs. Scale bar = 500 nm. **B** Representative size distribution of EVs derived from SKP-SCs detected by nanoparticle tracking analysis

(NTA). **C** Evaluation of EVs markers (CD81, Alix and TSG101) and non-EV markers (Calnexin) in SKP-SC-EVs by Western blot. SKP-SC was used as the control

2.3 Animals and Surgical procedure

Sprague–Dawley (SD) rats (220–250 g) were from the Animal Center of Nantong University. Rat experiments were performed following the institutional animal care guidelines of Nantong University. Totally 20 rats were utilized in the experiment and randomized into two groups before surgery (10 rats in each group), including the NG (chitosan nerve graft) and EV-NG (chitosan nerve graft incorporated with SKP-SC-EVs) groups. The rats were intraperitoneally injected with compound anesthetics at a dosage of 0.35 ml/100 g body weight, which contained 42.5 and 8.86 mg/ml chloral hydrate and pentobarbital sodium, respectively. The right sciatic nerve was exposed and cut to leave a 15-mm-long defect upon nerve retraction. After nerve transection, the NG was implanted with a thread-containing 8–0 suture needle and 1 mm of the nerve stump was advanced into the lumen, followed by suture to the nerve conduit. In the EV-NG group, SKP-SC-EVs (2×10^{10} particles in 16 μ l PBS) and Matrigel were mixed at 1:1 (v/v), administered by injection into a chitosan nerve conduit, and incubated at 37 °C for 30 min for Matrigel

solidification. After surgery, all the animals were administered daily celecoxib doses (20 mg/kg for 7 days) intragastrically to avoid inflammation and relieve pain.

2.4 Behavioral analysis

Motor and sensory function recoveries were analyzed by gait analysis and the plantar test at 6-, 8-, 10- and 12 postoperative weeks with the protocol described previously [23]. For gait analysis, parameters such as print length, intermediary toe spread and toe spread were obtained with CatWalk XT 9.0 (Noldus Information Technology, Wageningen, The Netherlands) to calculate Sciatic Function Index (SFI) values [25]. SFI values range from -100 to 0 , with “ 0 ” representing normal function, and “ -100 ” suggesting total dysfunction. For the plantar test, after environment adaption in a separate Plexiglas box, rats were stimulated with a radiant heat flux, and the withdrawal time of the right hind paw was recorded for evaluating heat hypersensitivity and sensory function recovery of the damaged hind limb.

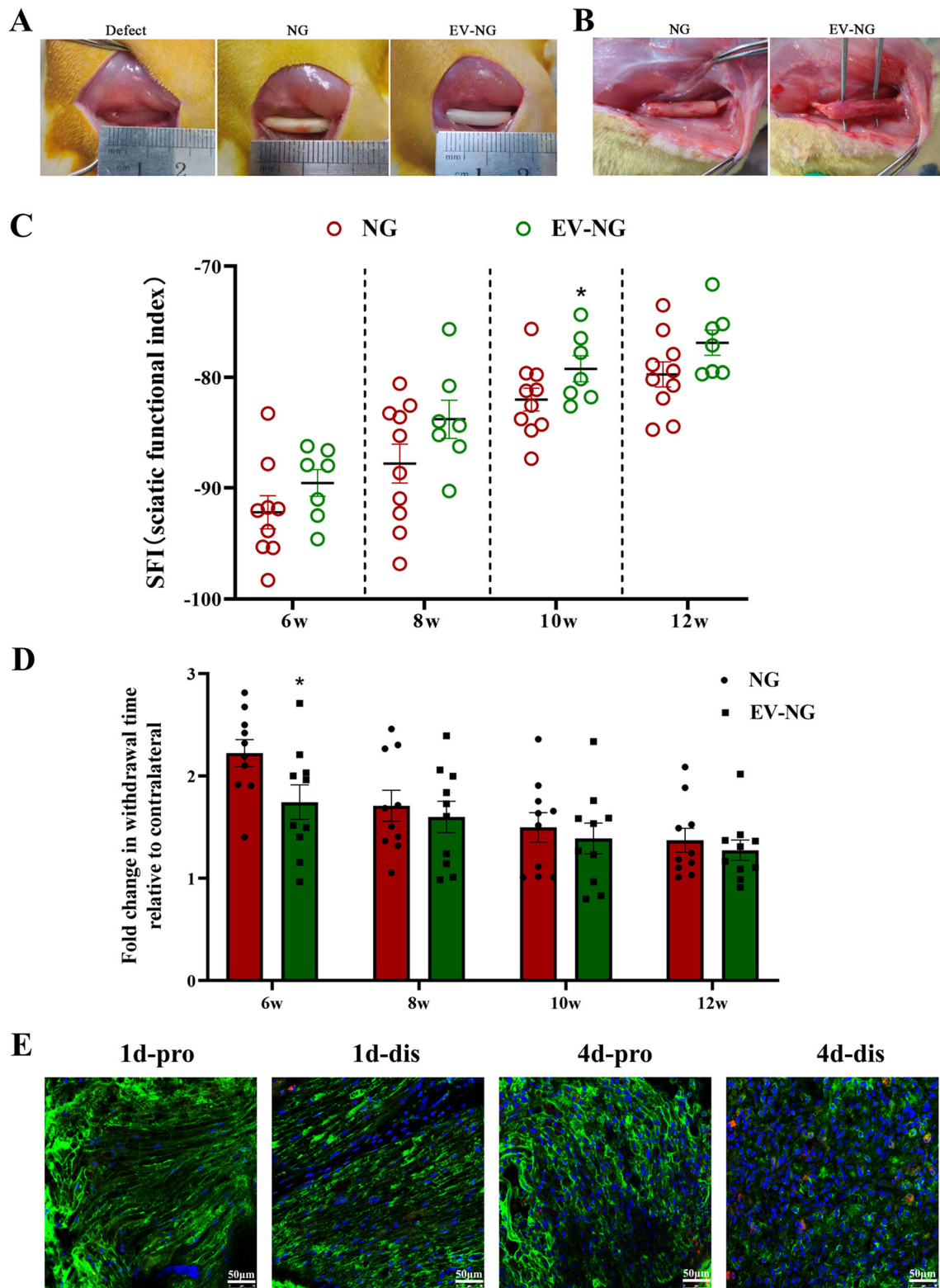


Fig. 2 Behavioral recovery with nerve graft implanted into sciatic nerve defect in rats. **A** Photographs showing the surgery after sciatic nerve defect (15 mm) in rats. An artificial nerve graft (NG) or NG incorporated with SKP-SC-EVs (EV-NG) was implanted into a 15 mm sciatic nerve defect. **B** Gross view of the regenerated nerve at 12 weeks after implantation in the NG group and EV-NG group. **C** At 6-, 8-, 10- and 12-weeks post-surgery, the SFI values of rats implanted with NG or EV-NG were measured with CatWalk gait analysis ($n = 10$ in NG group and $n = 7$ in EV-NG group). **D** At 6-, 8-, 10- and 12-postoperative weeks, the withdrawal time in response to thermal stimulation in each group was detected by the plantar test ($n = 10$ in each group and 3 times were performed with an interval of 10 min for each animal). All data are presented as mean \pm SEM. * $p < 0.05$ with unpaired Student's *t*-test (two-sided). **E** Confocal microscopy photographs showing the uptake of PKH26-labeled SKP-SC-EVs (red) by SCs (green, S100 positive) in the proximal (pro) and distal (dis) nerve stumps at 1 d and 4 d post-surgery. The nucleus was stained with DAPI. Scale bar = 50 μ m

2.5 Labeling of SKP-SC-EVs *in vivo*

To evaluate the *in vivo* delivery of SKP-SC-EVs, PKH26-labeled SKP-SC-EVs were used in the transplantation procedure as described above. At 1 postoperative day and 4 postoperative days, the animals were perfused and fixed with 4% paraformaldehyde (PFA). The frozen cutting sections of the nerve stumps were immunostained with the marker of Schwann cells (S100) and nucleus (DAPI) to evaluate the *in vivo* cellular uptake of SKP-SC-EVs.

2.6 Fluorogold retrograde tracing

At 11 postoperative weeks, the damaged sciatic nerve was re-exposed, and 5% FluorogoldTM (FG) was administered by injection into the nerve trunk at the site about 5 mm from the distal end of the nerve graft. Rats were transcranially perfused with 4% PFA 1 week later, and lumbar spinal cord segments and L4–6 dorsal root ganglions (DRGs) were collected for post-fixation. The obtained spinal cord and DRG specimens underwent serial sectioning on a cryostat at 30 and 20 μ m, respectively, followed by staining with Hoechst 33,258. The micrographs were acquired by confocal microscopy, and the percentages of FG-positive spinal cord motor neurons and DRG sensory neurons were assessed.

2.7 Electrophysiological evaluation

Functional recovery of sciatic nerve conduction was assessed via electrophysiological examinations at 12 postoperative weeks. The detailed protocol referred to a previously described method [26]. Briefly, anesthesia was followed by right sciatic nerve exposure and compound muscle action potential (CMAP) recording with a Keypoint

electrophysiological recorder (Alpine BioMed ApS, Skovlunde, Denmark).

2.8 Immunofluorescent staining

After behavioral analysis and electrophysiological recording, rats underwent perfusion and fixation with 4% PFA. The sciatic nerves and target muscles, including tibialis anterior (TA), gastrocnemius (GC), and soleus (Sol) muscles, were utilized to prepare frozen sections. Immunofluorescent staining was performed routinely. The sciatic nerve sections underwent overnight incubation with primary antibodies targeting S100 (1:200) and NF200 (1:200) at 4 °C, after which the samples were incubated with Alexa Fluor 594- and Alexa Fluor 488-linked anti-rabbit IgG at ambient for 2 h. Counterstaining was carried out with Hoechst 33,258. The muscles were stained with anti-Laminin antibodies (1:500) overnight at 4 °C followed by incubation with secondary antibodies. The neuromuscular junction (NMJ) was shown in longitudinal muscle sections co-stained with α -BTX (1:200) and anti-NF200 (1:200). Image acquisition utilized an SP5 confocal microscope (Leica, Wetzlar, Germany) and assessed with Image J 1.8.0 (National Institutes of Health, Bethesda, MD, USA).

2.9 Quantitative reverse transcription polymerase chain reaction (qRT-PCR)

At 12 postoperative weeks, the regenerated sciatic nerves of each group were harvested and the total RNA was extracted with TRIzol reagent (Invitrogen, USA). Total RNA was reversely transcribed to cDNA with an Omniscript RT kit and qRT-PCR was performed with SYBR green mix to measure the mRNA expressions of growth-associated protein 43 (*Gap43*), myelin protein zero (*Mpz*), and myelin basic protein (*Mbp*). The forward and reverse primers used for qRT-PCR analysis are listed below: *Gap43* (tgaggagaagaaggcgaagg; aggacggcgagtatcagtgtag); *Mpz* (aggctctcaggtggtggtcatc; ggcgttcttgaggctggttcac); *Mbp* (ttgatggtctgaagctcgtc; caaagaataactggcagggtg); *GAPDH* (acaccgacctcaccatct; tctctgctcctccctgttc). *GAPDH* was used as the internal control. Data were normalized to *GAPDH* and then quantified relative to the expressions in the NG group.

2.10 Transmission electron microscopy (TEM)

At 12 postoperative weeks, sciatic nerve and TA muscle samples from the injured side underwent fixation with 4% PFA and 0.5% glutaraldehyde. Sections for TEM were prepared and images were taken with a TEM (Hitachi, Japan) as previously described [23]. The thicknesses of

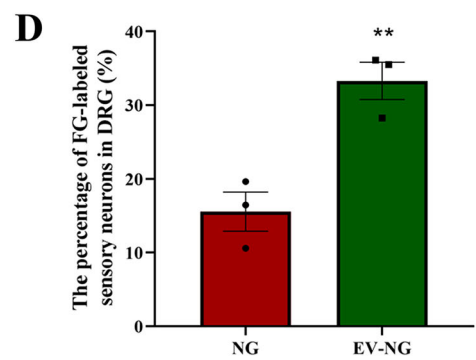
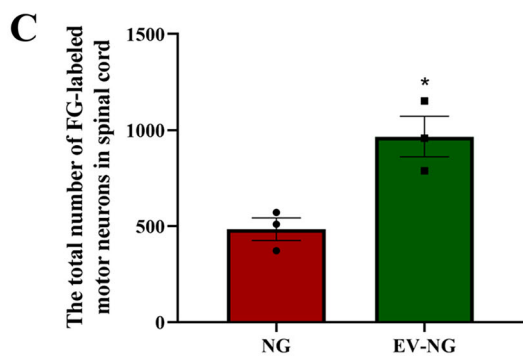
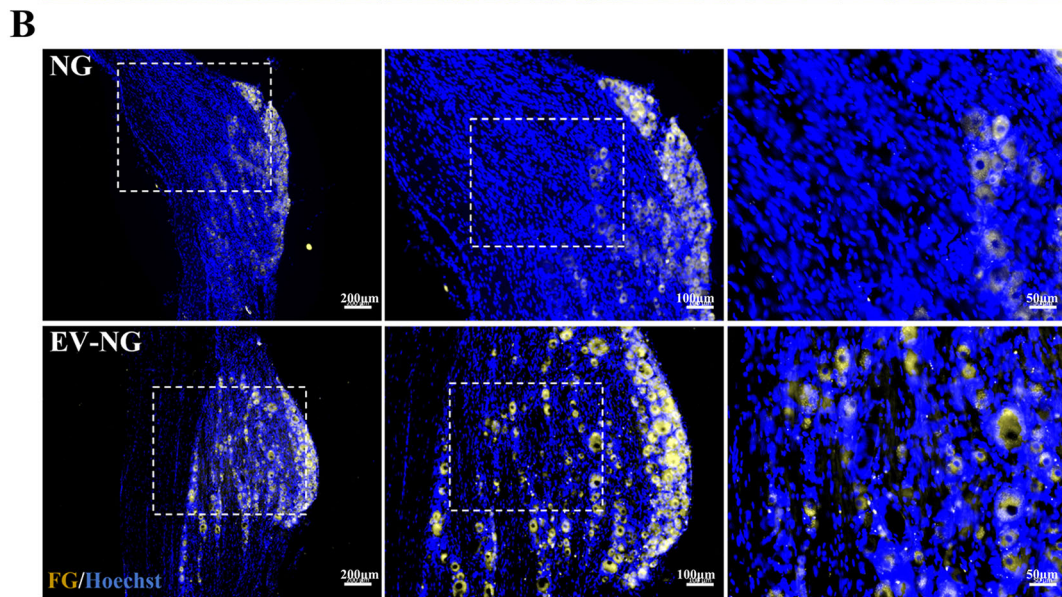
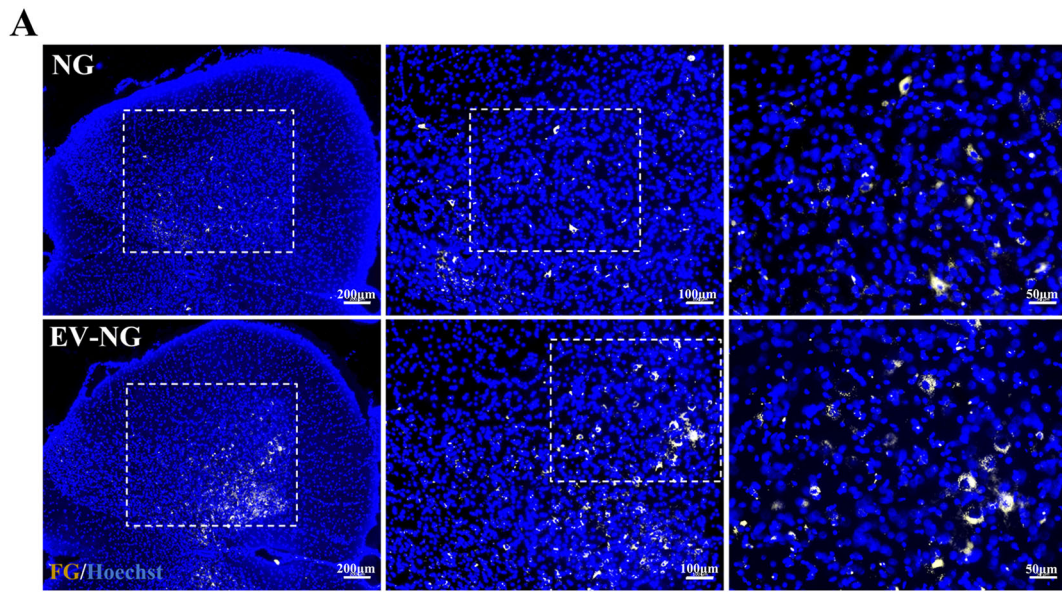


Fig. 3 Fluorescence photomicrographs of neurons retrogradely labeled with Fluorogold (FG) on the ipsilateral side of surgery. **A** Representative images of FG-labeled motor neurons (golden) in the spinal cord at 12 postoperative weeks. Scale bar = 200 μm (left), 100 μm (middle), and 50 μm (right). The nucleus was stained with Hoechst (blue). **B** Representative image of FG-labeled sensory neurons (golden) in the DRGs at 12 postoperative weeks. Scale bar = 200 μm (left), 100 μm (middle), and 50 μm (right). The nucleus was stained with Hoechst (blue). **C** Comparison of the percentage of FG-labeled motor neurons in the spinal cord between the NG group and EV-NG group ($n = 3$ in each group). **D** Comparison of the percentage of FG-labeled sensory neurons in the DRGs between the NG group and EV-NG group ($n = 3$ in each group). All data are presented as mean \pm SEM. * $p < 0.05$, ** $p < 0.01$ with unpaired Student's t -test (two-sided)

myelin sheaths, the diameters of myelinated nerve fibers, and myelin lamella amounts were quantified with Image J.

2.11 Histopathological analysis

At 12 postoperative weeks, the wet weights of TA, GC, and Sol muscles from the damaged and contralateral sides were measured right after collection, followed by fixation with 4% PFA and dehydration with an ethanol gradient. 5- μm transverse tissue sections were subjected to Masson's trichrome staining and image acquisition utilizing a microscope (Leica). Cross-sectional areas for TA, GC, and Sol muscle samples were calculated with the Image J software.

2.12 Statistical analysis

Statistical analysis was carried out with GraphPad Prism 8.2.1 (GraphPad Software Inc., La Jolla, CA, USA). Data are mean \pm SEM. Two-sided unpaired Student's t -test was carried out for between-group comparisons. $p < 0.05$ indicated statistical significance.

3 Results

3.1 Characterization of SKP-SC-EVs

To characterize the SKP-SC-EVs, TEM, NTA, and Western blot were performed to investigate the morphology, particle size, and expression of EVs marker proteins. The TEM image displayed the typical cup-shaped morphology of EVs (Fig. 1A). The NTA showed that the diameter of the SKP-SC-EVs ranged from 95 to 262 nm with an average diameter of 179 nm (Fig. 1B). Western blot analysis showed that several marker proteins of EVs, including CD81, Alix, and TSG101, were highly expressed in the SKP-SC-EVs, while the non-EV marker protein, Calnexin, was not expressed in the SKP-SC-EVs (Fig. 1C).

3.2 General features of the regenerated sciatic nerve

The gross view of a 5-mm sciatic nerve defect in the rat model is shown in Fig. 2A, and the defects were bridged with a chitosan nerve graft (NG) and an SKP-SC-EVs-incorporating chitosan nerve graft (EV-NG), respectively. The regenerated nerves were assessed at 12 postoperative weeks. No significant neuroma formation and inflammation were observed after nerve graft transplantation. Nerve defects were successfully bridged with nerve-like tissue by nerve graft implantation, and the regenerated nerve-like tissue had reduced thickness in the NG group in comparison with the EV-NG group (Fig. 2B).

3.3 Chitosan nerve grafts incorporated with SKP-SC-EVs enhance functional recovery of the sciatic nerve

Gait analysis showed that SFI values in both groups increased with time, showing motor function recovery after nerve graft transplantation (Fig. 2C). Although SFI values were elevated in the EV-NG group compared with the NG group at each time point, the difference was significant only at 10 postoperative weeks (Fig. 2C). To evaluate the sensory function recovery of the animals, the plantar test was performed. Withdrawal times in rats after thermal stimulation decreased with time after transplantation in both groups and were starkly shortened in the EV-NG group compared with the NG group at 6 postoperative weeks (Fig. 2D), indicating a better sensory function recovery with EV-NG implantation. Behavioral analysis indicated that incorporating SKP-SC-EVs in chitosan nerve grafts might improve the motor and sensory function recoveries of damaged sciatic nerves.

3.4 Chitosan nerve grafts incorporated with SKP-SC-EVs promote sciatic nerve regeneration

Immunostaining showed that PKH26-labeled SKP-SC-EVs co-localized with S100 positive SCs in the proximal and distal stumps of injured sciatic nerve, indicating that the transplanted SKP-SC-EVs could be taken up by the residual SCs *in vivo* (Fig. 2E).

Fluorogold retrograde tracing was applied to reveal the connection between the nerve stumps and the retrograde transportation of the regenerated nerves. FG-labeled motor and sensory neurons were detected in lumbar spinal cord segments and L4–6 dorsal root ganglions (DRGs) at the injured side at 12 postoperative weeks in both the NG and EV-NG groups (Fig. 3A). The percentages of FG-labeled motor neurons (Fig. 3B) and sensory neurons (Fig. 3B) were both markedly elevated in the EV-NG group.

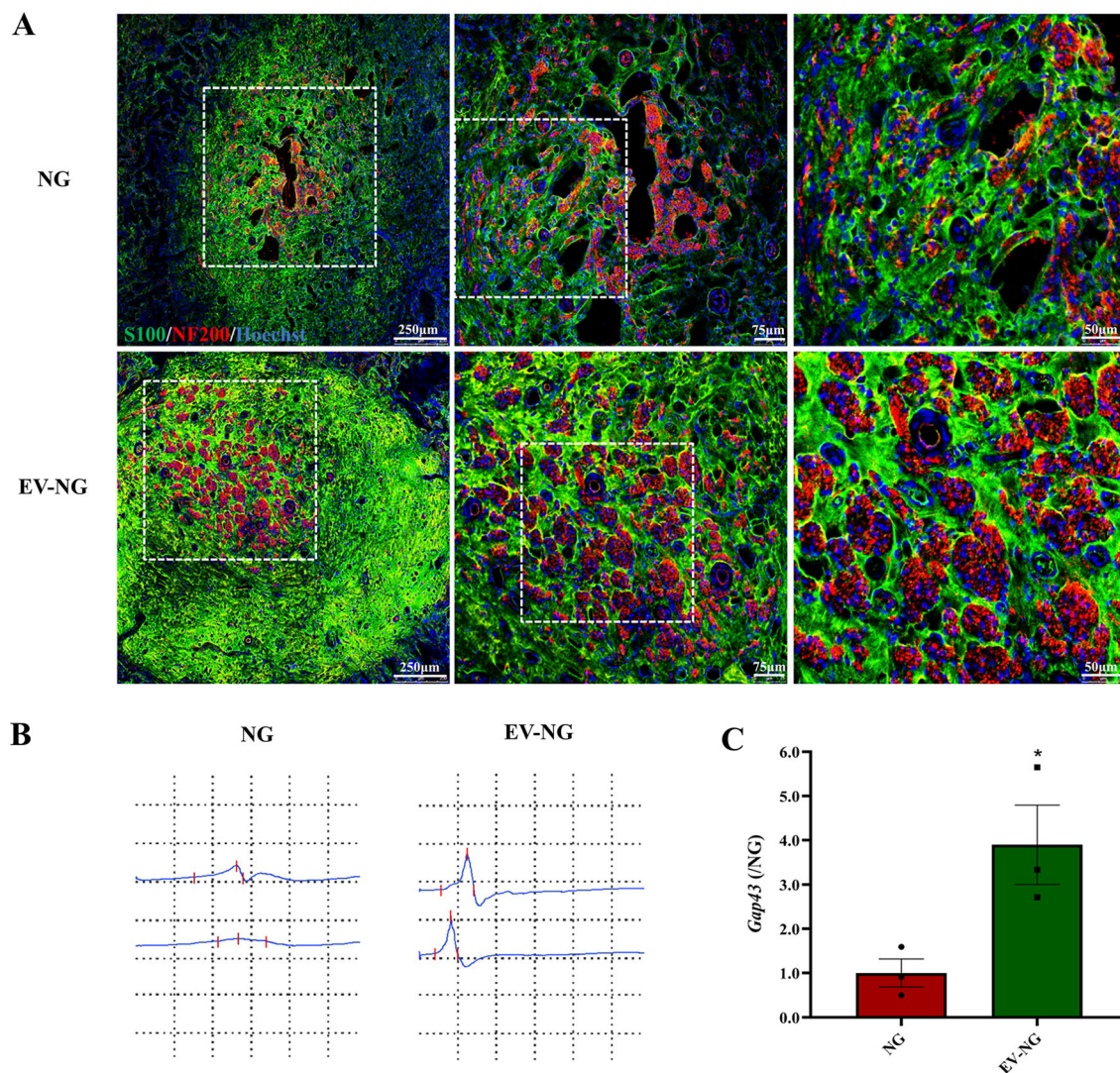
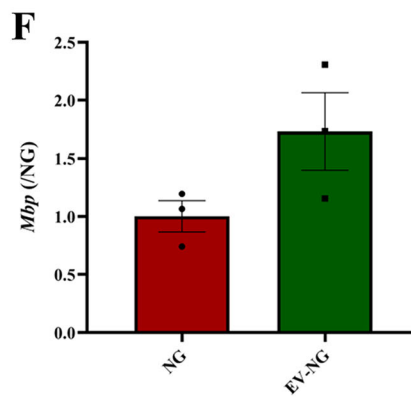
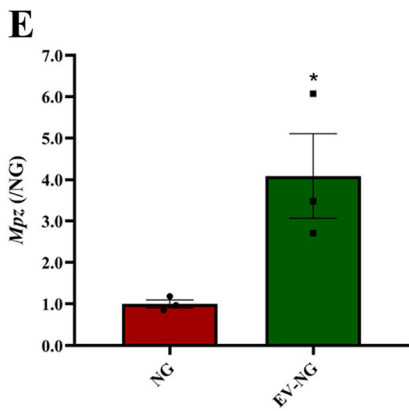
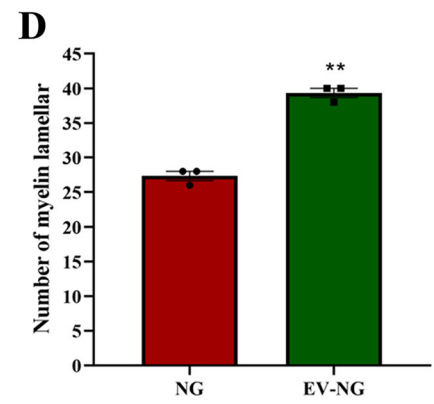
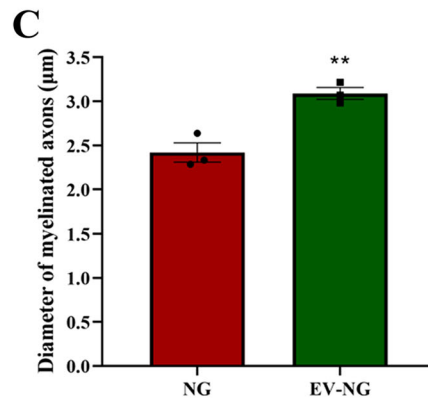
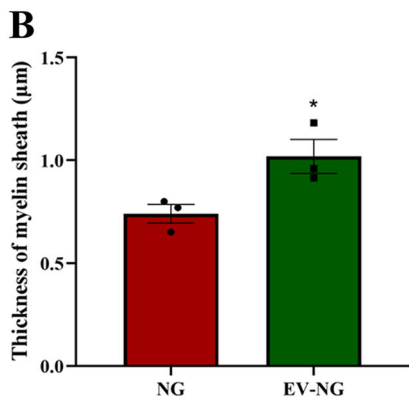
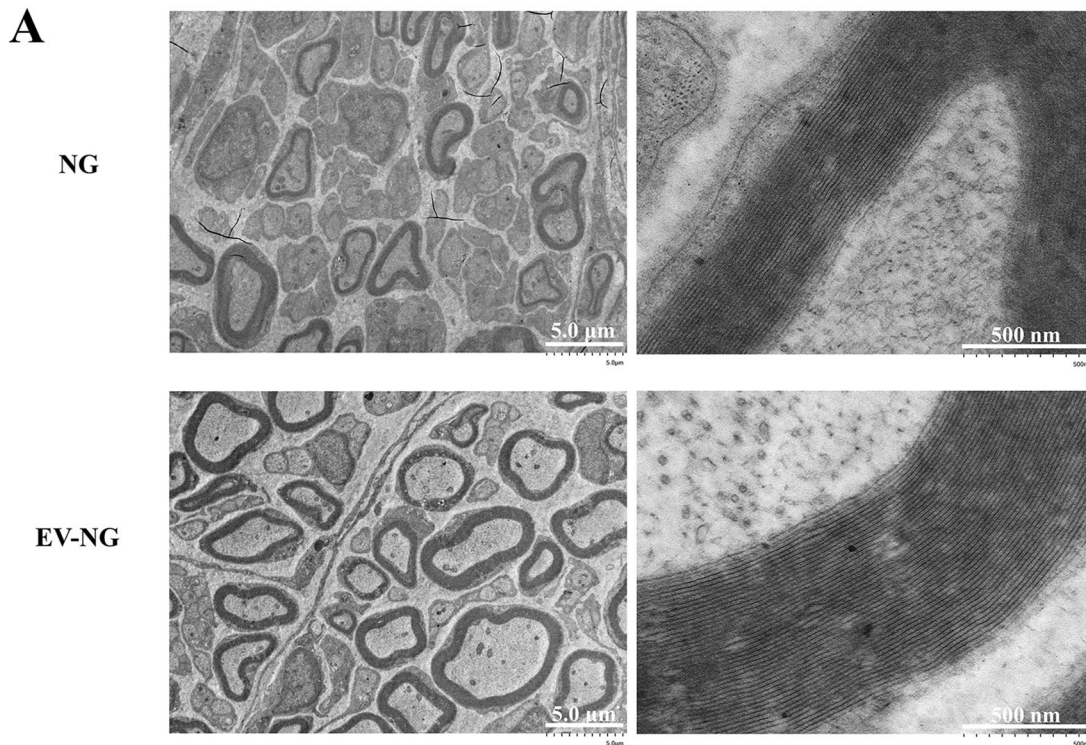


Fig. 4 Morphological and functional analysis of regenerated nerves. **A** At 12 postoperative weeks, immunofluorescent staining images of the cross-sections from the middle portion of the sciatic nerve were taken by a Leica confocal microscope. The myelin sheath was stained with S100 (Green) and axons with NF200 (red). The nucleus was shown with Hoechst 33,258 staining (blue). Scale bar = 250 μm (left), 75 μm (middle), and 25 μm (right). **B** Representative CMAP

images of the sciatic nerve were recorded at 12 weeks post implantation of NG or EV-NG with an intensity of 1 mA. **C** The expression of *Gap43* in the regenerated nerves measured by qRT-PCR ($n = 3$ in each group). The expression in the NG group was arbitrarily taken as 1. All data are presented as mean \pm SEM. $*p < 0.05$ with unpaired Student's *t*-test (two-sided)

To observe the morphological features of the regenerated nerve fibers, immunostaining was carried out on the transverse sections of the regenerated nerves. Axons were stained with NF200, and SCs underwent staining with S100, showing myelin sheaths around the regenerated axons in both groups. The fluorescence intensities of NF200 and S100, as well as nerve fiber density in the EV-NG group, were markedly elevated compared with the NG group (Fig. 4A). Electrophysiological recordings showed stimulated CMAP in the EV-NG group while no CMAP was recorded in the NG group (Fig. 4B). In addition, the gene related to axon regeneration, *Gap43*, increased significantly in the EV-NG group (Fig. 4C). These evidence

Fig. 5 Remyelination of regenerated nerves. **A** Representative TEM images of the regenerated sciatic nerve fibers at 12 weeks post implantation of NG or EV-NG. Scale bars = 5 μm (left) and 500 nm (right). Comparison of **B** the thickness of myelin sheath, **C** the diameter of myelinated axons, and **D** the number of myelin lamellar of regenerated nerve fibers between NG group and EV-NG group ($n = 3$ in each group and 5 random fields per rat was calculated for each group). **E, F**, The expression of *Mpz* and *Mbp* in the regenerated nerves measured by qRT-PCR ($n = 3$ in each group). The expression in the NG group was arbitrarily taken as 1. All data are presented as mean \pm SEM. $*p < 0.05$, $**p < 0.01$ with unpaired Student's *t*-test (two-sided)



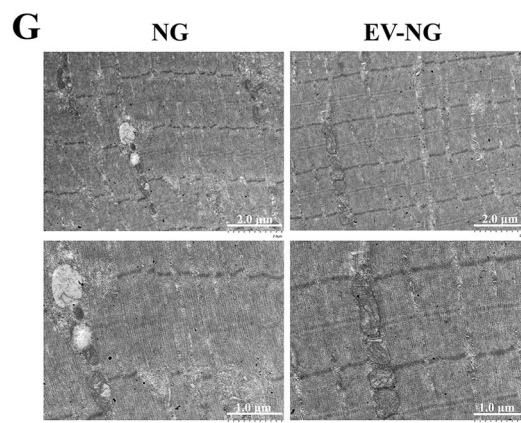
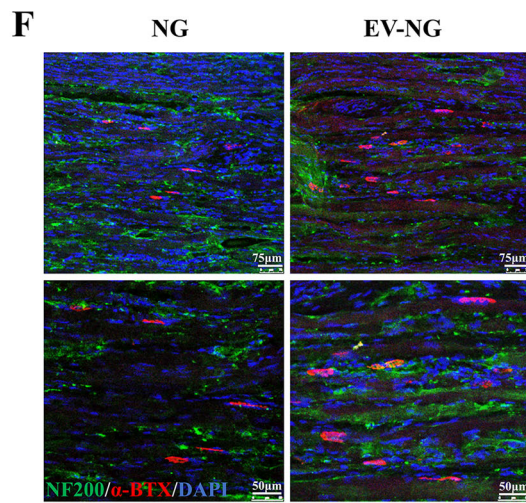
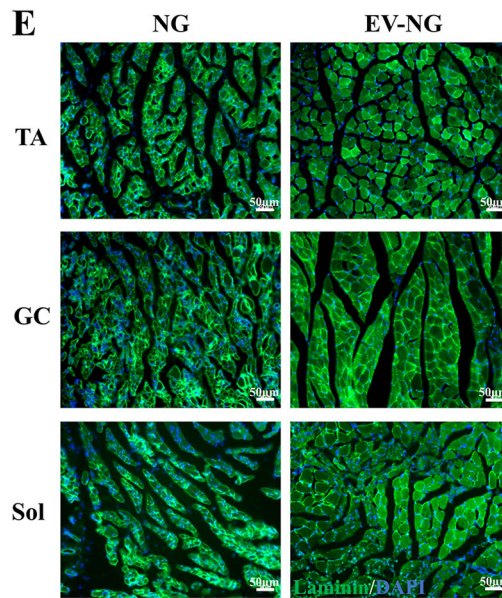
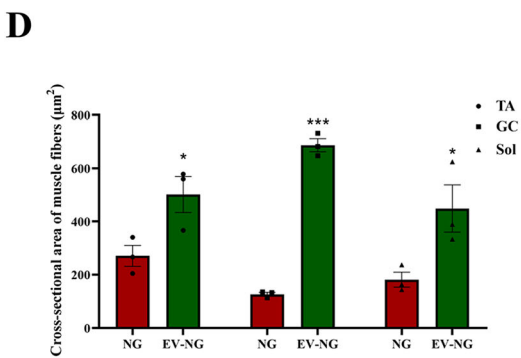
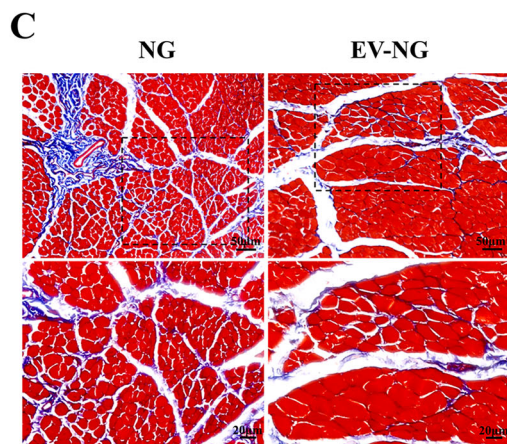
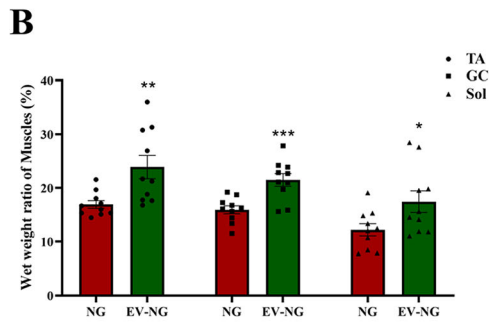
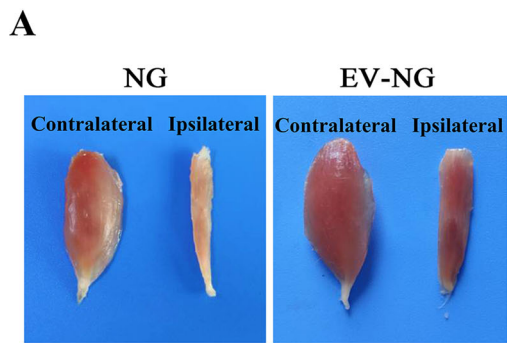


Fig. 6 Morphological and functional analysis of target muscles. **A** Gross view of the TA muscles in different groups at 12 postoperative weeks. **B** Comparison of the wet weight ratios (ipsilateral injured side/contralateral uninjured side) of TA, GC, and Sol muscles between the NG group and EV-NG group ($n = 10$ in each group). **C** Representative images of Masson's trichrome staining of cross-sections of TA muscles on the injured side. Scale bar = 50 μm . **D** Comparison of the cross-sectional area of TA, GC, and Sol muscles between the NG group and EV-NG group ($n = 3$ in each group and 5 random fields per rat was calculated for each group). **E** Representative images of laminin (green) immunostaining of TA, GC, and Sol muscles on the injured side. Scale bar = 50 μm . The nucleus was stained with DAPI (blue). **F** Representative images of α -BTX staining (red) in the longitudinal sections of TA muscles showing NMJs. The nerve fibers were stained with NF200 (green) and the nucleus with DAPI staining (blue). Scale bar = 75 μm . **G** Representative TEM images of TA muscles in the NG group and EV-NG group. Scale bar = 2 μm (upper) and 1 μm (lower). Data are presented as mean \pm SEM. * $p < 0.05$, ** $p < 0.01$, *** $p < 0.001$ with unpaired Student's t -test (two-sided)

indicated the presence of regenerated axon fibers in the EV-NG group.

To further analyze the remyelination of regenerated nerve fibers at the ultrastructural level, TEM was performed, and the acquired images showed dispersed unmyelinated and myelinated nerve fibers in the regenerated nerves in both groups (Fig. 5A). The thicknesses of myelin sheaths (Fig. 5B), the diameters of myelinated nerve fibers (Fig. 5C), and myelin lamella numbers (Fig. 5D) were all markedly higher in the EV-NG group in comparison with the NG group. The expression of *Mpz* (Fig. 5E) and *Mbp* (Fig. 5F) was also increased in the regenerated nerves of EV-NG group, although the difference of *Mbp* was not significant due to the large individual differences between each animal. The above data suggested that the incorporation of SKP-SC-EVs into chitosan NGs promoted sciatic nerve regeneration and enhanced myelination in regenerated axons.

3.5 Chitosan nerve grafts incorporated with SKP-SC-EVs inhibit muscle atrophy

Nerve defects often induce muscular atrophy due to denervation. At 12 postoperative weeks, TA, GC, and Sol muscles were harvested for morphological and histological assessments. TA muscles from the ipsilateral side of injured sciatic nerves showed overt atrophy in comparison with the contralateral side in both groups; however, atrophy seemed to have higher severity in the NG group versus the EV-NG group (Fig. 6A). The wet weight ratio of the ipsilateral sides to the contralateral sides of TA, GC, and Sol muscles also showed significant increases in the EV-NG group (Fig. 6B). Masson's trichrome staining revealed reduced amounts of collagen fibers (blue) and larger

muscle cells (red) in the EV-NG group (Fig. 6C), and average cross-sectional areas for TA, GC, and Sol muscles were starkly larger in the EV-NG group in comparison with the NG group (Fig. 6D). To further observe muscular atrophy in the above muscles, laminin immunostaining was performed. The results showed that the intensity of laminin fluorescence was much higher in the EV-NG group (Fig. 6E). NMJ staining with α -BTX revealed the amounts and areas of NMJ in the EV-NG group were larger than those of the NG group (Fig. 6F). Ultrastructural analysis of the TA muscle also displayed more clearly aligned myofilaments and Z-line in the EV-NG group, and the mitochondria were evenly distributed (Fig. 6G). The above data jointly indicated that the incorporation of SKP-SC-EVs could alleviate denervation-associated muscle atrophy.

4 Discussion

Repairing wide peripheral nerve defects is clinically challenging. Although NGCs composed of various synthetic or natural biomaterials could promote the functional recovery of peripheral nerves to some extent, the clinical outcomes remain insufficient in comparison with the application of the gold standard, autologous nerve transplantation. The potential reasons include an absence of supportive cells, downregulated neurotrophic factors, and degraded extracellular matrix, which compose the microenvironment for nerve regeneration [27, 28]. Thus, artificial nerve grafts incorporated with stem cells, neurotropic factors, and drugs are considered a promising substitute for autografts for long-distance PNI repair [16, 29].

SCs are ideal supportive cells promoting peripheral nerve regeneration. Unfortunately, their sources are limited, hindering the clinical application of SCs in PNI repair. In recent years, stem- or precursor cell-derived SCs have gradually become a research hotspot, especially those that could be easily obtained, including mesenchymal stem cells (MSCs), neural crest cells from keratinocytes (KCNCs) and the bone marrow (BM-NCCs), olfactory ecto-MSCs (OE-MSCs), human induced pluripotent stem cells (hiPSCs), adipose-derived stem cells (ADSCs) and skin-derived precursor cells (SKPs) [30–35]. The above cells could be differentiated into SCs and promote nerve regeneration, with great potential to be employed for clinically treating PNI. Our previous research successfully differentiated SKPs into a Schwann cell-like phenotype using heregulin-1 β and forskolin [24]. SKP-SCs were reported to remyelinate regenerated axons, improving behavioral recovery after nerve injury, by injection into acellular grafts [36]. In a tibial nerve injury model induced by doxorubicin, SKP-SCs could improve recovery in focal

nerve demyelination [37]. These findings indicated that SKP-SCs might be alternative supportive cells for peripheral nerve regeneration via the production of neuron growth factors and remyelination induction.

Although stem cells can differentiate into SCs and promote axonal regeneration, maintenance of cell viability, unwanted differentiation, and immunological problems constitute great challenges in their application [38]. To avoid these problems of cell-based therapies, cell-free therapies currently attract attention, especially EVs or exosomes released from SCs or stem cell-derived SCs. It was reported that exosomes from human adipose-derived MSCs (hADMSCs) regulate peripheral nerve-associated cell functions by preventing oxidative stress in SCs, inducing angiogenesis, and enhancing anti-inflammatory response [39]. Our previous work also demonstrated SKP-SC-derived EVs induce neurite outgrowth in sensory and motor neurons *in vitro*, and SKP-SCs incorporated into a silicone conduit could facilitate the repair of sciatic nerve defects in rats [23, 24, 40]. SKP-SC-EVs could also reduce denervation-related skeletal muscle atrophy by inhibiting oxidative stress and inflammatory response [41]. These findings suggest that the addition of EVs from various sources of SCs into NGs may constitute a promising strategy for PNI repair.

In this study, we used EVs derived from SKP-SCs and investigated their impact on nerve regeneration comparatively with nerve conduits without EVs in 15-mm nerve defects in a rat model. Behavioral analysis, morphological evaluation, molecular analysis and electrophysiological recording all demonstrated that the incorporation of SKP-SC-EVs promoted sciatic nerve regeneration and remyelination. Although the motor and sensory function recoveries only showed significant differences at 6 w and 10 w after transplantation, the data indicated that EVs might play important roles at the early stage of nerve regeneration. In addition, the structural integrity of NMJ and muscle fibers was also improved by EVs, suggesting muscle reinnervation can be achieved with nerve regeneration.

EVs may transfer a diversity of molecules, especially microRNAs (miRNAs), to regulate the expression of genes and their downstream pathways. MiR-21 carried by EVs derived from MSCs was found to be important in the regeneration process via PI3K/AKT signaling regulation and proliferation induction in SCs [42]. High expression of miR-21-5p was detected in SKP-SC-EVs, which could promote neuronal viability and attenuate neuronal apoptosis in oxygen-glucose-deprivation (OGD) injured dorsal root ganglions (DRGs) by negatively regulating PTEN-PI3K signaling [40]. Other miRNAs, such as miR-30a-5p, miR-19b, miR-29b-3p, miR-233, and miR-304-5p, were

equally found in SKP-SC-EVs, and their functions and target genes in peripheral nerve regeneration need further investigation.

In vivo delivery of EVs is another challenge hampering clinical application. In this study, we used chitosan as a scaffold and Matrigel, a thermo-responsive hydrogel, as a carrier system to transplant EVs in nerve defects. Chitosan is broadly utilized by tissue engineers for peripheral nerve reconstruction, with good biocompatibility and mechanical properties [43]. Additional cell seeding or supportive molecules like growth factors could promote nerve regeneration via chitosan-containing nerve conduits. Exosomes secreted by Schwann cell-like cells derived from human amniotic mesenchymal stem cells administered through an NT-3 chitosan conduit could promote sciatic nerve regeneration [44]. Chitosan scaffolds with prolonged controlled release of nerve growth factor were utilized for bridging 20-mm sciatic nerve defects in a rat model, long defects that are not easily overcome [39]. A 3D SC culture method utilizing Matrigel was developed to construct peripheral nerve conduits [45]. In addition, Matrigel-encapsulated cells or exosomes, e.g., SCs, vascular stem cells, ADSCs, and microvesicles of neural stem cells, are known to promote the functional recovery of PNI [46–49]. In this study, chitosan nerve conduits were applied to generate a microenvironment that promotes nerve regeneration, and the incorporated EVs derived from SKP-SCs might serve as a source of supportive molecules. Additionally, Matrigel might mediate a homogenous release of SKP-SC-EVs [23], thus facilitating the sustainable functions of EVs. However, in-depth studies are warranted to unveil the potential molecular mechanisms involved.

Together, we proved that EV-NG could markedly ameliorate motor and sensory function recovery compared with nerve conduits without EVs. Outgrowth and myelination in regenerated axons were induced, while the atrophy of target muscles induced by denervation was alleviated by the addition of EVs. These data indicated incorporation of SKP-SC-EVs into NGs might provide a promising method for repairing extended peripheral nerve damage.

Acknowledgements This study was supported by the National Natural Science Foundation of China (82201509), National Key Research and Development Program of China (Grant No. 2017YFA0104700), and the Priority Academic Program Development of Jiangsu High Education Institutions (PAPD).

Author contributions XYZ and MMY: experiment and manuscript drafting. XYZ, MMY, DYC, CYD and QZ: data analysis and figure preparation. XSG and FD: study design and manuscript revision. All authors approved the final manuscript.

Declarations

Conflict of interest The authors declare that the research was conducted in the absence of any commercial or financial relationships that could be construed as a potential conflict of interest.

Ethical Statement The animal study was reviewed and approved by the Administration Committee of Experimental Animals of institutional animal care guidelines of Nantong University (IACUC no. S20201025-003) and Jiangsu Province, China.

References

- Kornfeld T, Vogt PM, Radtke C. Nerve grafting for peripheral nerve injuries with extended defect sizes. *Wien Med Wochenschr.* 2019;169:240–51.
- Hercher D, Nguyen MQ, Dworak H. Extracellular vesicles and their role in peripheral nerve regeneration. *Exp Neurol.* 2022;350:113968.
- Patel NP, Lyon KA, Huang JH. An update-tissue engineered nerve grafts for the repair of peripheral nerve injuries. *Neural Regen Res.* 2018;13:764–74.
- Gu X, Ding F, Yang Y, Liu J. Construction of tissue engineered nerve grafts and their application in peripheral nerve regeneration. *Prog Neurobiol.* 2011;93:204–30.
- Pan J, Zhao M, Yi X, Tao J, Li S, Jiang Z, et al. Acellular nerve grafts supplemented with induced pluripotent stem cell-derived exosomes promote peripheral nerve reconstruction and motor function recovery. *Bioact Mater.* 2022;15:272–87.
- Eggers R, de Winter F, Tannemaat MR, Malessy MJA, Verhaagen J. GDNF gene therapy to repair the injured peripheral nerve. *Front Bioeng Biotechnol.* 2020;8:583184.
- Rao F, Wang Y, Zhang D, Lu C, Cao Z, Sui J, et al. Aligned chitosan nanofiber hydrogel grafted with peptides mimicking bioactive brain-derived neurotrophic factor and vascular endothelial growth factor repair long-distance sciatic nerve defects in rats. *Theranostics.* 2020;10:1590–603.
- Su Q, Nasser MI, He J, Deng G, Ouyang Q, Zhuang D, et al. Engineered Schwann cell-based therapies for injury peripheral nerve reconstruction. *Front Cell Neurosci.* 2022;16:865266.
- Chen S, Zhao Y, Yan X, Zhang L, Li G, Yang Y. PAM/GO/gel/SA composite hydrogel conduit with bioactivity for repairing peripheral nerve injury. *J Biomed Mater Res A.* 2019;107:1273–83.
- Zhang Z, Jorgensen ML, Wang Z, Amagat J, Wang Y, Li Q, et al. 3D anisotropic photocatalytic architectures as bioactive nerve guidance conduits for peripheral neural regeneration. *Biomaterials.* 2020;253:120108.
- Liu K, Yan L, Li R, Song Z, Ding J, Liu B, et al. 3D printed personalized nerve guide conduits for precision repair of peripheral nerve defects. *Adv Sci (Weinh).* 2022;9:2103875.
- Wei S, Hu Q, Ma J, Dai X, Sun Y, Han G, et al. Acellular nerve xenografts based on supercritical extraction technology for repairing long-distance sciatic nerve defects in rats. *Bioact Mater.* 2022;18:300–20.
- Kong Y, Xu J, Han Q, Zheng T, Wu L, Li G, et al. Electrospinning porcine decellularized nerve matrix scaffold for peripheral nerve regeneration. *Int J Biol Macromol.* 2022;209:1867–81.
- Rao F, Yuan Z, Li M, Yu F, Fang X, Jiang B, et al. Expanded 3D nanofibre sponge scaffolds by gas-foaming technique enhance peripheral nerve regeneration. *Artif Cells Nanomed Biotechnol.* 2019;47:491–500.
- Zhang D, Li Z, Shi H, Yao Y, Du W, Lu P, et al. Micropatterns and peptide gradient on the inner surface of a guidance conduit synergistically promotes nerve regeneration in vivo. *Bioact Mater.* 2022;9:134–46.
- Vijayavenkataraman S. Nerve guide conduits for peripheral nerve injury repair: A review on design, materials and fabrication methods. *Acta Biomater.* 2020;106:54–69.
- Zhao Y, Wang Y, Gong J, Yang L, Niu C, Ni X, et al. Chitosan degradation products facilitate peripheral nerve regeneration by improving macrophage-constructed microenvironments. *Biomaterials.* 2017;134:64–77.
- Jiang Z, Song Y, Qiao J, Yang Y, Zhang W, Liu W, et al. Rat sciatic nerve regeneration across a 10-mm defect bridged by a chitin/CM-chitosan artificial nerve graft. *Int J Biol Macromol.* 2019;129:997–1005.
- Meyer C, Stenberg L, Gonzalez-Perez F, Wrobel S, Ronchi G, Udina E, et al. Chitosan-film enhanced chitosan nerve guides for long-distance regeneration of peripheral nerves. *Biomaterials.* 2016;76:33–51.
- Makrygianni EA, Chrousos GP. Extracellular vesicles and the stress system. *Neuroendocrinology.* 2022. <https://doi.org/10.1159/000527182>.
- Kumar R, Sinha S, Hagner A, Stykel M, Raharjo E, Singh KK, et al. Adult skin-derived precursor Schwann cells exhibit superior myelination and regeneration supportive properties compared to chronically denervated nerve-derived Schwann cells. *Exp Neurol.* 2016;278:127–42.
- Zhu C, Huang J, Xue C, Wang Y, Wang S, Bao S, et al. Skin derived precursor Schwann cell-generated acellular matrix modified chitosan/silk scaffolds for bridging rat sciatic nerve gap. *Neurosci Res.* 2018;135:21–31.
- Yu M, Gu G, Cong M, Du M, Wang W, Shen M, et al. Repair of peripheral nerve defects by nerve grafts incorporated with extracellular vesicles from skin-derived precursor Schwann cells. *Acta Biomater.* 2021;134:190–203.
- Wu X, Wang L, Cong M, Shen M, He Q, Ding F, et al. Extracellular vesicles from skin precursor-derived Schwann cells promote axonal outgrowth and regeneration of motoneurons via Akt/mTOR/p70S6K pathway. *Ann Transl Med.* 2020;8:1640.
- Bain JR, Mackinnon SE, Hunter DA. Functional evaluation of complete sciatic, peroneal, and posterior tibial nerve lesions in the rat. *Plast Reconstr Surg.* 1989;83:129–38.
- Hu W, Yang M, Chang J, Shen Z, Gu T, Deng A, et al. Laser doppler perfusion imaging of skin territory to reflect autonomic functional recovery following sciatic nerve autografting repair in rats. *Microsurgery.* 2012;32:136–43.
- Yu T, Wen L, He J, Xu Y, Li T, Wang W, et al. Fabrication and evaluation of an optimized acellular nerve allograft with multiple axial channels. *Acta Biomater.* 2020;115:235–49.
- Yu T, Xu Y, Ahmad MA, Javed R, Hagiwara H, Tian X. Exosomes as a promising therapeutic strategy for peripheral nerve injury. *Curr Neuropharmacol.* 2021;19:2141–51.
- Meena P, Kakkar A, Kumar M, Khatri N, Nagar RK, Singh A, et al. Advances and clinical challenges for translating nerve conduit technology from bench to bed side for peripheral nerve repair. *Cell Tissue Res.* 2021;383:617–44.
- Podder AK, Mohamed MA, Tseropoulos G, Nasiri B, Andreadis ST. Engineering nanofiber scaffolds with biomimetic cues for differentiation of skin-derived neural crest-like stem cells to Schwann cells. *Int J Mol Sci.* 2022;23:10834.
- Shi H, Gong Y, Qiang L, Li X, Zhang S, Gao J, et al. Derivation of Schwann cell precursors from neural crest cells resident in bone marrow for cell therapy to improve peripheral nerve regeneration. *Biomaterials.* 2016;89:25–37.

32. Huang Z, Powell R, Phillips JB, Haastert-Talini K. Perspective on Schwann cells derived from induced pluripotent stem cells in peripheral nerve tissue engineering. *Cells*. 2020;9:2497.
33. Chen S, Ikemoto T, Tokunaga T, Okikawa S, Miyazaki K, Yamada S, et al. Newly generated 3D Schwann-like cell spheroids from human adipose-derived stem cells using a modified protocol. *Cell Transplant*. 2022;31:9636897221093312.
34. Entezari M, Mozafari M, Bakhtiyari M, Moradi F, Bagher Z, Soleimani M. Three-dimensional-printed polycaprolactone/polypyrrole conducting scaffolds for differentiation of human olfactory ecto-mesenchymal stem cells into Schwann cell-like phenotypes and promotion of neurite outgrowth. *J Biomed Mater Res A*. 2022;110:1134–46.
35. Horner SJ, Couturier N, Bruch R, Koch P, Hafner M, Rudolf R. hiPSC-Derived Schwann cells influence myogenic differentiation in neuromuscular cocultures. *Cells*. 2021;10:3292.
36. Khuong HT, Kumar R, Senjaya F, Grochmal J, Ivanovic A, Shakhbazov A, et al. Skin derived precursor Schwann cells improve behavioral recovery for acute and delayed nerve repair. *Exp Neurol*. 2014;254:168–79.
37. Grochmal J, Dhaliwal S, Stys PK, van Minnen J, Midha R. Skin-derived precursor Schwann cell myelination capacity in focal tibial demyelination. *Muscle Nerve*. 2014;50:262–72.
38. Fairbairn NG, Meppelink AM, Ng-Glazier J, Randolph MA, Winograd JM. Augmenting peripheral nerve regeneration using stem cells: a review of current opinion. *World J Stem Cells*. 2015;7:11–26.
39. Liu B, Kong Y, Shi W, Kuss M, Liao K, Hu G, et al. Exosomes derived from differentiated human ADMSC with the Schwann cell phenotype modulate peripheral nerve-related cellular functions. *Bioact Mater*. 2022;14:61–75.
40. Cong M, Shen M, Wu X, Li Y, Wang L, He Q, et al. Improvement of sensory neuron growth and survival via negatively regulating PTEN by miR-21-5p-contained small extracellular vesicles from skin precursor-derived Schwann cells. *Stem Cell Res Ther*. 2021;12:80.
41. Wang W, Shen D, Zhang L, Ji Y, Xu L, Chen Z, et al. SKP-SC-EVs mitigate denervated muscle atrophy by inhibiting oxidative stress and inflammation and improving microcirculation. *Antioxidants (Basel)*. 2021;11:66.
42. Ma Y, Zhou D, Zhang H, Tang L, Qian F, Su J. Human umbilical cord mesenchymal stem cell-derived extracellular vesicles promote the proliferation of Schwann cells by regulating the PI3K/AKT signaling pathway via transferring miR-21. *Stem Cells Int*. 2021;2021:1496101.
43. Boecker A, Daeschler SC, Kneser U, Harhaus L. Relevance and recent developments of Chitosan in peripheral nerve surgery. *Front Cell Neurosci*. 2019;13:104.
44. Chen W, Chang S, Yang C, Zhou J, Zhang H, Nie K, et al. Schwann cell-like cells derived from human amniotic mesenchymal stem cells promote sciatic nerve repair through an exosome-induced SOX2/FN1 pathway in vitro. *Int J Mol Med*. 2022;49.
45. Kim SM, Lee SK, Lee JH. Peripheral nerve regeneration using a three dimensionally cultured schwann cell conduit. *J Craniofac Surg*. 2007;18:475–88.
46. Cerqueira SR, Lee YS, Cornelison RC, Mertz MW, Wachs RA, Schmidt CE, et al. Decellularized peripheral nerve supports Schwann cell transplants and axon growth following spinal cord injury. *Biomaterials*. 2018;177:176–85.
47. Huang CW, Hsueh YY, Huang WC, Patel S, Li S. Multipotent vascular stem cells contribute to neurovascular regeneration of peripheral nerve. *Stem Cell Res Ther*. 2019;10:234.
48. Chen J, Ren S, Duscher D, Kang Y, Liu Y, Wang C, et al. Exosomes from human adipose-derived stem cells promote sciatic nerve regeneration via optimizing Schwann cell function. *J Cell Physiol*. 2019;234:23097–110.
49. Chen X, Ye K, Yu J, Gao J, Zhang L, Ji X, et al. Regeneration of sciatic nerves by transplanted microvesicles of human neural stem cells derived from embryonic stem cells. *Cell Tissue Bank*. 2020;21:233–48.

Publisher's Note Springer Nature remains neutral with regard to jurisdictional claims in published maps and institutional affiliations.

Springer Nature or its licensor (e.g. a society or other partner) holds exclusive rights to this article under a publishing agreement with the author(s) or other rightsholder(s); author self-archiving of the accepted manuscript version of this article is solely governed by the terms of such publishing agreement and applicable law.